

Topology and symmetry breaking in ABC trilayer graphene

Vladimir Cvetkovic¹ and Oskar Vafek¹

¹*National High Magnetic Field Laboratory and Department of Physics,
Florida State University, Tallahassee, FL 32306, USA*

(Dated: October 31, 2018)

The effects of topology and electron-electron interactions on the phase diagram of ABC stacked trilayer graphene (TLG) at the neutrality point are investigated within a weak coupling renormalization group approach. We find that the leading instability of TLG with only a forward scattering density-density interaction is towards a mirror-breaking gapless state. Addition of a small, but finite back scattering favors gapped phases, allowing us to make connections to the existing experiments on TLG. We identify a fundamental symmetry difference between TLG and bilayer graphene (BLG) which is responsible for disfavoring nematic states in TLG under the same conditions that favor nematic states in BLG.

Interest in the theory of metal-insulator transitions in divalent materials [1] has undergone a resurgence as of late in no small part due to the discovery of graphene [2–4]. There is growing experimental evidence for electron-electron (e-e) interaction-induced excitonic instabilities in AB stacked bilayer (BLG) [5–11] and the ABC stacked trilayer graphene (TLG) [12]. Theoretically, based on symmetry alone [1], TLG is qualitatively different from single layer graphene (SLG) and BLG. The valence band (VB) and the conduction band (CB) in SLG and BLG are members of the *same* irreducible representation (IR) of the symmetry group at the $\pm\mathbf{K} = \pm\frac{4\pi}{3\sqrt{3}a}\hat{\mathbf{x}}$ points in the Brillouin zone. On the other hand, the VB and the CB of TLG belong to *different* IR's such that the interband matrix element of the momentum operator vanishes at $\pm\mathbf{K}$.

SLG, BLG, and TLG are further distinguished in the topological character of their VB and the CB Bloch states as they wind along a closed \mathbf{k} -space loop around the $\pm\mathbf{K}$ points. Their winding numbers, which are 1, 2 and 3 respectively [13, 14], can be related to the experimentally measured steps in the quantized Hall conductivity as the carrier concentration is tuned from hole- to electron-like [3, 15, 16]. This non-trivial topology guarantees at least three Dirac Fermions (DF) near, but not exactly at, each of $\pm\mathbf{K}$ of BLG and TLG, placed along the 3-fold symmetry lines in the BZ. Since one can adjust the microscopic parameters of the model *without lowering the symmetry* so as to either rotate the three DF's or to introduce an additional six DF's near each $\pm\mathbf{K}$, the Dirac degeneracies in TLG cannot be established based on symmetry alone [17]. This raises the possibility of zero temperature phase transitions between different, but symmetry indistinguishable, thermodynamic phases.

In this work we systematically investigate the interplay of such topological effects and the e-e interactions in TLG. We employ a powerful theoretical machinery based on symmetry and renormalization group (RG), which leads us to the basic structure of the general phase diagram shown in Fig. 1 together with the list of, and the conditions for, the most dominant symmetry breaking

(SB) phases. As a biproduct, our symmetry analysis allows us to readily explain why 3-fold rotational SB gapless states in TLG considered recently within Hartree-Fock approximation are indeed unfavorable [18], unlike in BLG [19–22], while noting that there are 3-fold rotationally symmetric gapless states, not considered in Ref. 18, which break the mirror symmetry of the lattice and are stable in the limit of pure forward scattering. Nevertheless, small, *but finite* backscattering (i.e., intervalley scattering) makes gapless states unstable and promotes gapped phases. Our theory focuses from the outset on the most important low energy degrees of freedom and extends significantly beyond the recent functional RG treatment [23] that did not take into account RG relevant symmetry allowed terms and treated only up to nearest neighbor lattice interactions.

Because the experimentally observed [24] energy (few *meV*) scales associated with any ordering are small compared to the relevant band splitting scales (few 100's *meV*), the theory of the TLG needs to take into account only the modes which lie close to the Fermi level. The effective low energy Hamiltonian written in the vicinity of the $\pm\mathbf{K}$ points is

$$H = H_0 + H_{int}. \quad (1)$$

Setting $\hbar = k_B = 1$, the symmetry allowed terms in the non-interacting Hamiltonian are

$$H_0 = \sum_{\mathbf{k}, \sigma=\uparrow, \downarrow} \psi_{\mathbf{k}\sigma}^\dagger \left(h_{\mathbf{k}}^{A^+g} + h_{\mathbf{k}}^{A^+u} + h_{\mathbf{k}}^{A^+2u} \right) \psi_{\mathbf{k}\sigma}, \quad (2)$$

where $h_{\mathbf{k}}^{A^+g} = (-\epsilon_F + \frac{1}{2\delta m^*} \mathbf{k}^2) \mathbb{1}_4 + (\Delta + \frac{1}{2m^*} \mathbf{k}^2) \mathbb{1}_2 \sigma_1$, $h_{\mathbf{k}}^{A^+u} = R_1 k_x (k_x^2 - 3k_y^2) (R_0 \tau_3 \mathbb{1}_2 + \tau_3 \sigma_1)$ and $h_{\mathbf{k}}^{A^+2u} = R_2 k_y (3k_x^2 - k_y^2) \mathbb{1}_2 \sigma_2$. The Pauli matrices τ and σ act in the valley and layer space respectively. For each spin projection, the Fermi annihilation operators have been put into a four component vector $\psi_{\mathbf{k}\sigma} = (c_{\mathbf{k}+\mathbf{K}\sigma}^A, c_{\mathbf{k}+\mathbf{K}\sigma}^B, c_{\mathbf{k}-\mathbf{K}\sigma}^A, c_{\mathbf{k}-\mathbf{K}\sigma}^B)^T$ and $|\mathbf{k}| < \Lambda$ where $\Lambda \ll |\mathbf{K}|$. *A* and *B* refer to two undimerized sites on layers 1 and 3 (see Fig. 3 inset). There is some uncertainty in

the actual values and *signs* of the coefficients m^* and Δ [25–27]. In this Letter we choose $m^* > 0$ and sweep over a range of both positive and negative Δ 's. A situation where $m^* < 0$ can be mapped onto the $m^* > 0$ problem by simultaneous change in sign of m^* and Δ . Therefore, the results presented here cover every possible arrangement of parameter signs.

For $\Delta > \Delta_{c1} = 0$ there are three anisotropic DF's along three symmetry lines, and we label this state 3^+ (see Fig. 1). For $\Delta < \Delta_{c2} < \Delta_{c1}$ there are also three DF's but rotated by 180° relative to 3^+ . We label this state 3^- . For $\Delta_{c2} < \Delta < \Delta_{c1}$, and in the presence of *particle hole symmetry*, which we assume to hold from now on, $R_0 = 0$, and $1/\delta m^* = 0$, and the spectrum contains nine DFs; we label this state 9^- (see Fig. 1) [28]. Because at $T = 0$ it is impossible to transition between any two of 3^+ , 3^- , and 9^- states without encountering a non-analyticity in the ground state energy, even in this non-interacting case, there are two $T = 0$ quantum phase transitions. The transition at Δ_{c1} is 2^{nd} order and the one at $\Delta_{c2} = -1/(54(R_1)^2 m^{*3})$ is 3^{rd} order [29].

We find that, for arbitrarily small e-e interactions, the 2^{nd} order phase transition, initially at Δ_{c1} , is avoided and replaced by two continuous phase transitions into a spontaneously broken symmetry phase (see Fig. 1). The nature of the SB phase depends on the type and the strength of the e-e interactions and we discuss it in detail later in the text. On the other hand, the 3^{rd} order phase boundary point at Δ_{c2} turns into a critical line $\Delta_{c2}(g)$ for a finite range of weak interactions g , before it is terminated in quantum tricritical points.

We construct H_{int} using the irreducible representations (IR's) of the space symmetry group $P\bar{3}m1$ [30]. The most relevant scattering processes are described by the quartic contact terms. These are the products of two bilinears $g_{MN} (\psi_\alpha^\dagger(\mathbf{r})M_{\alpha\beta}\psi_\beta(\mathbf{r})) (\psi_\lambda^\dagger(\mathbf{r})N_{\lambda\rho}\psi_\rho(\mathbf{r}))$, where, neglecting the small spin-orbit coupling, the spin $SU(2)$ symmetry is assumed to be present, and so in the singlet channel $M_{\alpha\beta} = \tau_\mu\sigma_\nu\delta_{\alpha\beta}$ while in the triplet channel $M_{\alpha\beta} = \tau_\mu\sigma_\nu\vec{\sigma}_{\alpha\beta}$. Similar expressions hold for $N_{\lambda\rho}$ and $\mu, \nu = 0, 1, 2, 3$; (τ_0 or $\sigma_0 = \mathbb{1}_2$). When the quartic terms are integrated over \mathbf{r} , the symmetries of the lattice require that the product of two IR's to which M and N belong is the trivial IR. Further simplification comes from the fact that all the spin triplet-triplet terms can be written in terms of singlet-singlet terms using Fierz identities [21, 31]. Therefore, the most general contact quartic interaction terms preserving the time reversal symmetry, lattice symmetry, and spin $SU(2)$ symmetry are

$$H_{int} = \frac{4\pi}{|m^*|} \int d\mathbf{r} \left[\sum_{\mu\nu} g_{\mu\nu} \left(\sum_{\sigma} \psi_{\sigma}^{\dagger}(\mathbf{r})\tau_{\mu}\sigma_{\nu}\psi_{\sigma}(\mathbf{r}) \right)^2 \right. \\ \left. + 2 \sum_{\mu} \tilde{g}_{\mu} \sum_{\sigma, \sigma'} \left(\psi_{\sigma}^{\dagger}(\mathbf{r})\tau_{\mu}\mathbb{1}_2\psi_{\sigma}(\mathbf{r}) \right) \left(\psi_{\sigma'}^{\dagger}(\mathbf{r})\tau_{\mu}\sigma_1\psi_{\sigma'}(\mathbf{r}) \right) \right], \quad (3)$$

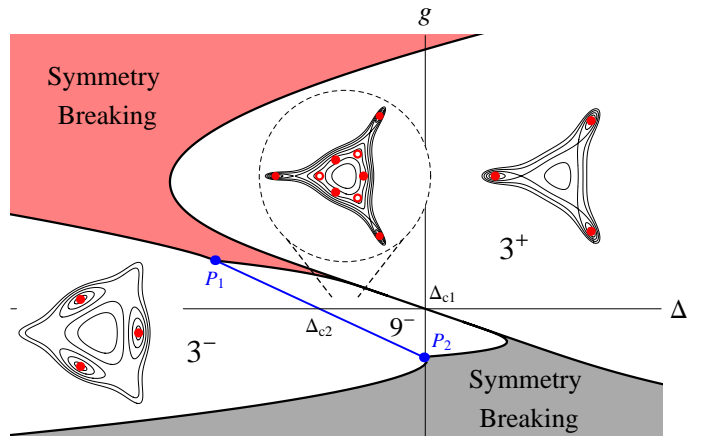


FIG. 1: Schematic zero temperature phase diagram for ABC stacked trilayer graphene at the neutrality point. g is the strength of the electron-electron interactions and Δ the conduction and valence band mixing at the symmetry points $\pm\mathbf{K}$ (see Eq. (2)). In the non-interacting case $\Delta_{c1, c2}$ mark the quantum phase transitions between distinct, but symmetry equivalent, states 3^+ , 9^- , and 3^- . Their schematic contours of constant energy near the \mathbf{K} point with Dirac points (red circles) are shown. The (blue) phase boundary between 3^- and 9^- terminates at two tricritical points P_1 and P_2 . At any finite g the direct transition between 3^+ and 9^- is avoided and replaced by transitions into a symmetry broken phase, whose width becomes exponentially small as $g \rightarrow 0$.

where $g_{1\nu} = g_{2\nu} \equiv g_{\mathbf{K}\nu}$, for each ν , and $\tilde{g}_1 = \tilde{g}_2 \equiv \tilde{g}_{\mathbf{K}}$, and we inserted the factor of $8\pi/|m^*|$, which makes g 's dimensionless, for convenience. The total number of independent, symmetry allowed, couplings is 15. We discuss the specific model choices of g 's further in the text.

To find the phase diagram, we evaluate the partition function $Z = \text{Tr} [e^{-H/T}]$ using coherent state path integrals and the Wilson renormalization group (RG) procedure [32] which, for BLG, has been spelled out in detail in Ref. 22. As the modes within the thin momentum shell $1 - d\ell < |\mathbf{k}|/\Lambda < 1$ and *any* Matsubara frequency $\omega_n = (2n + 1)\pi T$ are integrated out in powers of small g 's, the remaining modes, $\psi_{\mathbf{k}\sigma}^<(\omega_n)$ and their momenta are rescaled such that the new $|\mathbf{k}|$ cutoff is again Λ and we choose the coefficient of $\frac{\mathbf{k}^2}{2m^*}\sigma_1\mathbb{1}_2$ in $h_{\mathbf{k}}^{A\dagger g}$ to remain constant. To 1-loop order we obtain the following RG flow equations

$$\frac{d \ln t}{d\ell} = -2 \frac{d \ln r}{d\ell} = 2, \quad (4)$$

$$\frac{d\delta}{d\ell} = 2\delta + \sum_{\mu} \left[\tilde{g}_{\mu} \tilde{C}_{\mu} + \sum_{\nu} g_{\mu\nu} C_{\mu\nu} \Phi_0(t_{\ell}, \delta_{\ell}, r_{\ell}) \right], \quad (5)$$

$$\frac{d\tilde{g}_{\mu}}{d\ell} = \sum_{\alpha\beta} \sum_{\kappa\lambda\kappa'} \tilde{A}_{\mu(\alpha\beta)}^{\kappa\lambda, \kappa'} g_{\kappa\lambda} \tilde{g}_{\kappa'} \Phi^{(\alpha\beta)}(t_{\ell}, \delta_{\ell}, r_{\ell}), \quad (6)$$

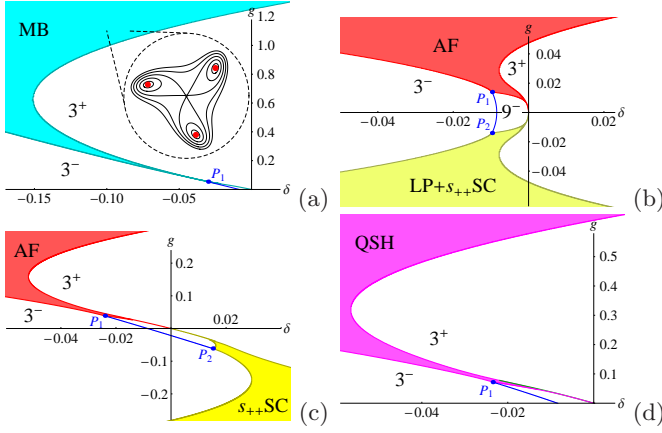


FIG. 2: $T = 0$ phase diagrams for the three interaction models for TLG studied here. (a) g_{00} -only, (b) weak coupling Hubbard model, (c+d) Screened Coulomb interaction.

$$\frac{dg_{\mu\nu}}{d\ell} = \sum_{\alpha\beta} \left[\sum_{\kappa\lambda\kappa'\lambda'} A_{\mu\nu(\alpha\beta)}^{\kappa\lambda,\kappa'\lambda'} g_{\kappa\lambda} g_{\kappa'\lambda'} + \sum_{\kappa\kappa'} \bar{A}_{\mu\nu(\alpha\beta)}^{\kappa\kappa'} \tilde{g}_{\kappa} \tilde{g}_{\kappa'} \right] \Phi^{(\alpha\beta)}(t_{\ell}, \delta_{\ell}, r_{\ell}), \quad (7)$$

where $t_{\ell=0} = T/\frac{\Delta^2}{2m^*}$, $\delta_{\ell=0} = \Delta/\frac{\Delta^2}{2m^*}$ and for simplicity we set $R_1 = R_2 = R$ in Eq. (2) giving $r_{\ell=0} = (2m^*\Lambda)R$. The expressions for the coefficients $C_{\mu\nu}$, \bar{C}_{μ} , A , \bar{A} , and \tilde{A} 's are too long to present here, but they are given in the Supplementary Material (SM). Φ functions are

$$\Phi_0(t, \delta, r) = \frac{T}{2} \sum_{\omega_n} \int_0^{2\pi} \frac{d\varphi}{2\pi} \text{Tr} [G_{\Lambda, \varphi}(\omega_n) \mathbb{1}\sigma_1], \quad (8)$$

$$\Phi^{(\mu\nu)}(t, \delta, r) = \frac{T}{16} \sum_{\omega_n} \int_0^{2\pi} \frac{d\varphi}{2\pi} (\text{Tr} [G_{\Lambda, \varphi}(\omega_n) \tau_{\mu}\sigma_{\nu}])^2 \quad (9)$$

In the above, the one particle Greens function, given by $G_{\mathbf{k}}^{-1}(\omega_n) = -i\omega_n + h_{\mathbf{k}}^{A_{1g}^+} + h_{\mathbf{k}}^{A_{1u}^-} + h_{\mathbf{k}}^{A_{2u}^-}$, is evaluated at the circle $|\mathbf{k}| = \Lambda$ parameterized by φ .

While the details of the flow described by the above equations must be solved numerically, the general trends can be readily understood. From Eq. (4), $t_{\ell} = t_{\ell=0}e^{2\ell}$ and $r_{\ell} = r_{\ell=0}e^{-\ell}$. Starting from some fixed initial values of g 's and sufficiently high temperature $t_{\ell=0}$, the exponential decay of the Φ 's with growing ℓ quickly halts the growth of the magnitude of the g 's, which saturate to finite values as $\ell \rightarrow \infty$. Such a flow corresponds to a phase with no spontaneous SB. Holding the values of the initial g 's fixed and reducing $t_{\ell=0}$, there is an increase in the values of ℓ where Φ 's halt the flow, and the limiting magnitude of the g 's increases as $\ell \rightarrow \infty$. Whether the g 's eventually diverge upon further lowering of $t_{\ell=0}$ depends on the initial values of the remaining parameters. The highest $t_{\ell=0}$ at which g 's diverge as $\ell \rightarrow \infty$ is identified with the critical temperature t_c . At t_c , the growth of the magnitude of the g 's is precisely balanced by the decay in

the Φ 's. We do not extend our calculations below t_c . For the parameters corresponding to phases 3^+ , 3^- and 9^- in Fig. 1, the g 's remain finite as $\ell \rightarrow \infty$ even if $t_{\ell=0} = 0$.

Since $\Phi_0 \neq 0$ for $\delta = 0$, a finite δ is generated under RG even if we set the mixed couplings $\tilde{g}_{\mu} = 0$ as we assume later on. This is similar to the 1-loop renormalization of the mass (or transition temperature) in bosonic ϕ^4 theory [33], and is ultimately responsible for the slanted shape of the phase boundaries in Fig. 1 near small g .

To extract physical information about the nature of the SB we calculate the ordering susceptibilities, χ_i^C , for a large number of excitonic, i.e., particle-hole (p-h), and superconducting, i.e., particle-particle (p-p) channels C . The C =p-h considered are $\sum_{\alpha\beta} \int d^2\mathbf{r} \psi_{\alpha}^{\dagger}(\mathbf{r}) O_{\alpha\beta}^i \psi_{\beta}(\mathbf{r})$, where $O^i = \tau_{\mu}\sigma_{\nu}\delta_{\alpha\beta}$ for singlet, and $O^i = \tau_{\mu}\sigma_{\nu}\vec{\sigma}_{\alpha\beta}$ for triplet channels. The C =p-p considered are $\frac{1}{2} \sum_{\alpha\beta} \int d^2\mathbf{r} \psi_{\alpha}(\mathbf{r}) \tilde{O}_{\alpha\beta}^i \psi_{\beta}(\mathbf{r}) + h.c.$. The χ_i^C can be calculated using the methods detailed in Ref. [22] and for TLG it is given by

$$\chi_i^C = \frac{|m^*|}{8\pi} \int_0^{\infty} d\ell \sum_{\mu\nu} \alpha_{i(\mu\nu)}^C e^{2\Omega_i^C(\ell)} \Phi^{(\mu\nu)}(t_{\ell}, \delta_{\ell}, r_{\ell}). \quad (10)$$

where

$$\Omega_i^C(\ell) = \sum_{\mu\nu\mu'\nu'} B_{i,(\mu'\nu')}^{C,\mu\nu} \int_0^{\ell} d\ell' g_{\mu\nu}(\ell') \Phi^{(\mu'\nu')}(t_{\ell'}, \delta_{\ell'}, r_{\ell'}), \quad (11)$$

and constants $\alpha_{i,(\mu\nu)}^C$ and $B_{i,(\mu'\nu')}^{C,\mu\nu}$ are given in the SM. The above equations hold in the absence of the mixed couplings, i.e., $\tilde{g}_{\mu} = 0$. This holds at the bare level in any of the model cases we studied in detail. Moreover, if absent, \tilde{g}_{μ} is not generated by Eq. (6). In each case our numerical evaluations of the RG flow equations and the χ_i^C 's benefited from additional analytical study of the flow at asymptotically large ℓ near t_c . We were able to enumerate all stable flow trajectories (rays) and determine the instabilities and exponents for each of these.

Model 1: Fig. 2a shows the phase diagram in the forward scattering limit, i.e., only $g_{00}(\ell = 0) \neq 0$. The system exhibits an excitonic (p-h) instability in the spin-singlet $\tau_3\sigma_2$ channel. This SB term belongs to A_{2g}^+ IR: it breaks lattice *mirror* symmetries and C_2' rotations (180° rotations about the axes perpendicular to principal 3-fold axes). It does *not* break the 3-fold rotational symmetry about the principal axes [34], inversion, or time reversal symmetry. We call this mirror-breaking (MB) phase. The spectrum inside the MB phase is gapless with DP's rotated in the same direction at each $\pm K$ valley. Our calculations indicate that MB is very sensitive to the presence of even very small back scattering terms, $g_{\mathbf{K}3}/g_{00}$ and $g_{\mathbf{K}0}/g_{00} \gtrsim 4 \times 10^{-3}$, in which case gapped phases are preferred (See Fig. 3).

Model 2: The results for the Hubbard model are presented in Fig. 2b. In this case the initial couplings in Eq. (3) are $g_{03} = g_{00} \sim U$, $g_{\mathbf{K}0} = g_{\mathbf{K}3} = \frac{1}{2}g_{00}$ and all other

couplings vanish initially. Due to the $SO(4)$ symmetry of the Hubbard model [22, 35–37], the phase boundary has the same shape for repulsive and attractive on-site interaction U . In the former case, $U > 0$, we find the leading excitonic instability to be $O_i = \mathbb{1}_2 \sigma_3 \vec{\sigma}$, i.e., a layer antiferromagnet (AF) [23] whose electronic spectrum is gapped. AF breaks time reversal and inversion symmetry. In the latter case, $U < 0$, the leading instability is found to be equally strong for $O_i = \mathbb{1}_2 \sigma_3 \mathbb{1}_2$ i.e., a spontaneously layer-polarized (LP) state and $\hat{O}_i = \tau_1 \mathbb{1}_2 \sigma_2$ i.e., an s_{++} -superconducting state (SC). The LP breaks inversion and the SC the charge $U(1)$ symmetry. Their spectrum is also gapped. Just as in the case of BLG, a mapping connecting these flows can be found [22]. At the transition into the AF phase, all g 's diverge along the AF stable ray (see the SM). Due to the $SO(4)$ symmetry, the asymptotic flow corresponding to the LP+SC instability can be obtained from the AF stable ray. This is an unstable fixed ray in the g -space and is a consequence of fine tuning. An infinitesimally small interaction that breaks the $SO(4)$ symmetry results either in LP only or SC only instability. Numerically, we see this as a diversion of the flow toward one of two distinct stable fixed rays corresponding to these phases.

Model 3: Finally, we consider cases of interaction most likely to capture the situation in the experiments where e-e interaction is screened due split-off bands and gates: backscattering is finite, but small compared to g_{00} . This makes $g_{\mathbf{K}3} = g_{\mathbf{K}0}$. In the phase diagram, Fig. 2c, we set $g_{\mathbf{K}0}/g_{00} = 0.1$ as a representative value. Changing this ratio does not induce qualitative changes as we show later in Fig. 3. When $g_{00} > 0$ the leading instability is towards AF, the flow following the same stable ray as in the case of the Hubbard model. For $g_{00} < 0$, the leading instability is towards s_{++} -SC. The phase diagram in the case of attractive back scattering (here represented by $g_{\mathbf{K}0}/g_{00} = -0.1$) is shown in Fig. 2d. For the major part of the transition line, we find that the model undergoes a transition to a SB phase with $O_i = \tau_3 \sigma_3 \vec{\sigma}$, i.e., (gapped in bulk) quantum spin Hall phase (QSH) [23]. Only in a small portion of the phase boundary ($g_{00} \lesssim 0.04$) facing the 3^+ phase the leading instability changes to $O_i = \tau_1 \sigma_3 \mathbb{1}_2$ or $O_i = \tau_2 \sigma_3 \mathbb{1}_2$, the two order parameters being equivalent by lattice symmetry. This instability leads to the layer polarization density wave (LPDW), a state where both top and bottom layers exhibit a charge density wave, but the local density of charge has opposite sign on the two layers. The spectrum of the LPDW phase is gapless.

It is easy to understand why spontaneous rotational SB phases are unfavorable in TLG. Because the low energy degrees of freedom in TLG reside on the sites directly above/below each other in the two outer layers, the 120° rotations have no effect on the valley-layer matrices $\tau_\mu \sigma_\nu$. Therefore, any rotational SB order parameter operator must involve at least one power of \mathbf{k} , making it less rel-

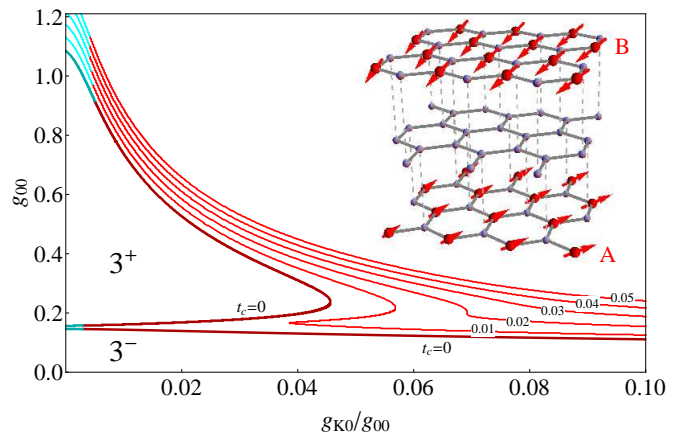


FIG. 3: The influence of back scattering on the transition temperature and symmetry breaking channel. The color of isotherms corresponds to the leading instability: mirror-breaking (cyan), anti-ferromagnet (red). In 3^\pm regions no symmetry breaking occurs, even at $T = 0$. Inset: a TLG lattice with the AF order.

evant under RG, and therefore less likely to condense, than the \mathbf{k} -independent operators considered here. This is unlike in BLG, where the two sites are horizontally displaced, some $\tau_\mu \sigma_\nu$ transform non-trivially under rotations, and such states can be favored [19, 22].

In Fig. 3 we examine the influence of back scattering on the transition temperature and the leading instability. We choose to use non-interacting Hamiltonian parameters [27] that yield $\Lambda = 0.106/a$, $r_0 = 4.19$, and $\delta_0 = -0.071$, as only for $\delta < 0$, the TLG phase diagram may exhibit reentrant SB phase (see Fig. 2a). The relative strength of back to forward scattering, $g_{\mathbf{K}0}/g_{00}$, varies from 0 to 0.1, therefore connecting the left and right edges of this plot to Figs. 2a and c, respectively. With no back scattering and at finite T , the critical interaction g_{00} at which the MB phase sets in must be fairly large. A presence of non-zero $g_{\mathbf{K}0}$ quickly suppresses this value, implying that the back scattering helps to enhance T_c . The MB instability is suppressed by back scattering, too, with the AF order preferred whenever $g_{\mathbf{K}0}/g_{00} \gtrsim 4 \times 10^{-3}$. This result suggests that the gapped state observed in TLG experiments [24] is most probably the AF state (Fig. 3 inset).

The authors acknowledge discussions with B. Roy in the early stages of this work and thank R.E. Throckmorton for a critical reading of the manuscript. This work was supported by the NSF CAREER award under Grant No. DMR-0955561, NSF Cooperative Agreement No. DMR-0654118, and the State of Florida.

[1] B.I. Halperin and T.M. Rice, Solid State Phys. **21**, 115 (1968); Rev. Mod. Phys. **40**, 755 (1968).

- [2] K.S. Novoselov, A. K. Geim, S.V. Morozov, D. Jiang, Y. Zhang, S.V. Dubonos, I.V. Grigorieva, A.A. Firsov, *Science* **306**, 666 (2004).
- [3] K.S. Novoselov, A.K. Geim, S.V. Morozov, D. Jiang, M.I. Katsnelson, I.V. Grigorieva, S.V. Dubonos, and A.A. Firsov, *Nature* **438**, 197 (2005).
- [4] Y. Zhang, Y.-W. Tan, H.L. Stormer, and P. Kim, *Nature* **438**, 201 (2005).
- [5] R.T. Weitz, M.T. Allen, B.E. Feldman, J. Martin, and A. Yacoby, *Science* **330**, 812 (2010).
- [6] J. Martin, B.E. Feldman, R.T. Weitz, M.T. Allen, and A. Yacoby, *Phys. Rev. Lett.* **105**, 256806 (2010).
- [7] A.S. Mayorov, D.C. Elias, M. Mucha-Kruczyński, R.V. Gorbachev, T. Tudorovskiy, A. Zhukov, S.V. Morozov, M.I. Katsnelson, V.I. Fal'ko, A.K. Geim, and K.S. Novoselov, *Science* **333**, 860 (2011).
- [8] J. Velasco Jr., L. Jing, W. Bao, Y. Lee, P. Kratz, V. Aji, M. Bockrath, C.N. Lau, C.M. Varma, R. Stillwell, D. Smirnov, F. Zhang, J. Jung, and A.H. MacDonald, *Nat. Nanotech.* **7**, 156 (2012).
- [9] A. Veligura, H.J. van Elferen, N. Tombros, J.C. Maan, U. Zeitler, and B.J. van Wees, *Phys. Rev. B* **85**, 155412 (2012).
- [10] F. Freitag, J. Trbovic, M. Weiss, and C. Schönenberger, *Phys. Rev. Lett.* **108**, 076602 (2012).
- [11] W. Bao, J. Velasco Jr., F. Zhang, L. Jing, B. Standley, D. Smirnov, M. Bockrath, A. MacDonald, and C.N. Lau, *Proc. Natl. Acad. Sci. USA* **109**, 10802 (2012).
- [12] W. Bao, L. Jing, J. Velasco Jr, Y. Lee, G. Liu, D. Tran, B. Standley, M. Aykol, S.B. Cronin, D. Smirnov, M. Koshino, E. McCann, M. Bockrath, and C.N. Lau, *Nat. Phys.* **7**, 948 (2011).
- [13] E. McCann, V.I. Fal'ko, *Phys. Rev. Lett.* **96**, 086805 (2006), and references therein.
- [14] M. Koshino, and E. McCann, *Phys. Rev. B* **80**, 165409 (2009).
- [15] K.S. Novoselov, E. McCann, S.V. Morozov, V.I. Fal'ko, M.I. Katsnelson, U. Zeitler, D. Jiang, F. Schedin, A.K. Geim, *Nat. Phys.* **2**, 177 (2006).
- [16] L. Zhang, Y. Zhang, J. Camacho, M. Khodas, and I. Zaliznyak, *Nat. Phys.* **7**, 953 (2011).
- [17] In principle, sufficiently large *symmetry preserving* terms may even completely remove the three DF's by moving them from \mathbf{K} across the Brillouin zone and annihilating them with DF's from $-\mathbf{K}$ along the symmetry lines.
- [18] J. Jung, and A.H. MacDonald, arXiv:1208.0116v1 (unpublished).
- [19] O. Vafek, and K. Yang, *Phys. Rev. B* **81**, 041401 (2010).
- [20] Y. Lemonik, I.L. Aleiner, C. Toke, and V.I. Fal'ko, *Phys. Rev. B* **82**, 201408 (2010).
- [21] Y. Lemonik, I.L. Aleiner, and V.I. Fal'ko, *Phys. Rev. B* **85**, 245451 (2012).
- [22] V. Cvetkovic, R.E. Throckmorton, and O. Vafek *Phys. Rev. B* **86**, 075467 (2012) .
- [23] M.M. Scherer, S. Uebelacker, D.D. Scherer, and C. Honerkamp, arXiv:1208.5323 (unpublished).
- [24] W. Bao, L. Jing, J. Velasco Jr, Y. Lee, G. Liu, D. Tran, B. Standley, M. Aykol, S.B. Cronin, D. Smirnov, M. Koshino, E. McCann, M. Bockrath, and C.N. Lau, *Nat. Phys.* **7**, 948 (2011).
- [25] J.C. Slonczewski, and P.R. Weiss, *Phys. Rev.* **109**, 272 (1958); J.W. McClure, *Phys. Rev.* **108**, 612 (1957);
- [26] B. Partoens, and F.M. Peeters, *Phys. Rev. B* **74**, 075404 (2006).
- [27] F. Zhang, B. Sahu, H. Min, and A.H. MacDonald, *Phys. Rev. B* **82**, 035409 (2010).
- [28] In the absence of particle hole symmetry 9^- would correspond to a compensated semimetal with particle and hole Fermi surfaces.
- [29] The order of the transition refers to the Ehrenfest classification, i.e., it is labeled by the lowest derivative of the free energy with respect to the tuning parameter Δ which is discontinuous at the transition.
- [30] S. Latil, and L. Henrard, *Phys. Rev. Lett.* **97**, 036803 (2006).
- [31] O. Vafek, *Phys. Rev. B* **82**, 205106 (2010).
- [32] R. Shankar, *Rev. Mod. Phys.* **66**, 129 (1994).
- [33] H. Kleinert and V. Schulte-Frohlinde *Critical Properties of ϕ^4 -Theories* (World Scientific Publishing, River Edge, NJ), (2001).
- [34] Therefore the mirror symmetry breaking state should not be confused with Nematic.
- [35] C.N. Yang, *Phys. Rev. Lett.* **63**, 2144 (1989).
- [36] S.C. Zhang, *Phys. Rev. Lett.* **65**, 120 (1990).
- [37] C.N. Yang, S.C. Zhang, *Mod. Phys. Lett. B* **4**, 759 (1990).

SUPPLEMENTARY MATERIAL

SYMMETRIES IN ABC TRILAYER GRAPHENE AND IRREDUCIBLE REPRESENTATION CLASSIFICATIONS

The space group of ABC trilayer graphene (TLG) lattice symmetries is $P\bar{3}m1$. The lattice is invariant under translations by any vector $\mathbf{R} = m_{+1}\hat{b}_{+1} + m_{-1}\hat{b}_{-1}$, where $m_{\pm 1}$ are integers, and $\hat{b}_{\pm 1} = a\sqrt{3}/2\hat{x} \pm 3a/2\hat{y}$ are the unit vectors of the lattice. At Γ -point, the point group of lattice symmetries is \mathbf{D}_{3d} ; at other high symmetry points of relevance to graphene, $\pm\mathbf{K}$, the point group of lattice symmetries is \mathbf{D}_3 . The character tables for these two point groups are given in Table I.

\mathbf{D}_{3d}	e	$2C_3$	$3C_2'$	i	$2S_6$	$3\sigma_d$
A_{1g}	1	1	1	1	1	1
A_{2g}	1	1	-1	1	1	-1
E_g	2	-1	0	2	-1	0
A_{1u}	1	1	1	-1	-1	-1
A_{2u}	1	1	-1	-1	-1	1
E_u	2	-1	0	-2	1	0

\mathbf{D}_3	e	$2C_3$	$3C_2'$
A_1	1	1	1
A_2	1	1	-1
E	2	-1	0

TABLE I: Character tables for groups \mathbf{D}_{3d} and \mathbf{D}_3 .

In addition to obeying the lattice symmetries, we want our Hamiltonian, Eq. (1) in the main text, to be invariant under the time reversal, and under the group of global $SU(2)$ spin rotations. The $SU(2)$ spin rotation invariance is implemented by taking a general Dirac bilinear $\sum_{\alpha=\uparrow,\downarrow} \psi_{\alpha}^{\dagger} M_{\alpha\beta} \psi_{\beta}$, and noticing that it is a spin-singlet when $M = \tau_{\mu}\sigma_{\nu}\delta_{\alpha\beta}$, while it is a spin-triplet for $M = \tau_{\mu}\sigma_{\nu}\vec{\sigma}_{\alpha\beta}$. The non-interacting part of the Hamiltonian may contain only spin-singlet Dirac bilinears, while the interaction part may have either a product of two spin-singlet or a scalar product of two spin-triplet bilinears.

The tensors formed by the remaining two matrices, $\tau_{\mu}\sigma_{\nu}$, are classified according to the irreducible representation (IR) of the space group they transform under:

$$\begin{aligned}
 A_{1g,\Gamma}^{+} : \mathbb{1}_4, \mathbb{1}\sigma_1; & \quad A_{2g,\Gamma}^{+} : \tau_3\sigma_2; & \quad A_{2g,\Gamma}^{-} : \tau_3\sigma_3; & \quad A_{1u,\Gamma}^{-} : \tau_2\mathbb{1}, \tau_3\sigma_1; & \quad A_{2u,\Gamma}^{+} : \mathbb{1}\sigma_3; & \quad A_{2u,\Gamma}^{-} : \mathbb{1}\sigma_2; \\
 A_{1,\pm\mathbf{K}}^{+} : (\tau_1 \pm i\tau_2)\mathbb{1}, (\tau_1 \pm i\tau_2)\sigma_1; & \quad A_{2,\pm\mathbf{K}}^{+} : (\tau_1 \pm i\tau_2)\sigma_3; & \quad A_{2,\pm\mathbf{K}}^{-} : (\tau_1 \pm i\tau_2)\sigma_2. & & &
 \end{aligned} \tag{12}$$

The superscripts in the names of IR's denote whether an M component is even (+) or odd (-) under time reversal.

The momentum operators and symmetric tensors they form (up to third order) are classified according to the IR's, too:

$$\begin{aligned}
 A_{1g,\Gamma}^{+} : |\mathbf{k}|^0 = 1, \quad |\mathbf{k}|^2 = k_x^2 + k_y^2; & \quad A_{1u,\Gamma}^{-} : |\mathbf{k}|^3 \cos 3\varphi_{\mathbf{k}} = k_x(k_x^2 - 3k_y^2); & \quad A_{2u,\Gamma}^{-} : |\mathbf{k}|^3 \sin 3\varphi_{\mathbf{k}} = k_y(k_y^2 - 3k_x^2); \\
 E_{g,\Gamma}^{+} : |\mathbf{k}|^2 e^{\pm i2\varphi_{\mathbf{k}}} = (k_x^2 - k_y^2) \pm i(2k_x k_y); & \quad E_{u,\Gamma}^{-} : |\mathbf{k}| e^{\pm i\varphi_{\mathbf{k}}} = k_x \pm ik_y, & \quad |\mathbf{k}|^3 e^{\pm i\varphi_{\mathbf{k}}} = (k_x^2 + k_y^2)(k_x \pm ik_y). &
 \end{aligned} \tag{13}$$

All Dirac bilinears in TLG belong to one-dimensional IR's. Therefore, they are allowed to appear in a term of the non-interacting Hamiltonian, Eq. (2) in the main text, only if multiplied by the momentum tensor belonging to the same IR as the bilinear.

β -FUNCTION COEFFICIENTS

Here we present the expressions for coefficients appearing in Eqs. (5-7), (10), and (11) in the main text. The coefficients appearing in the flow of δ , Eq. (5) in the main text, are

$$C_{\mu\nu} = 2\text{Tr} \left((\sigma_1 \sigma_{\nu})^2 \right) - 32\delta_{\mu 0} \delta_{\nu 1}, \quad \text{and} \quad \tilde{C}_{\mu} = 8 - 32\delta_{\mu 0}. \tag{14}$$

Each coefficient A in Eq. (7) in the main text has contributions due to random phase approximation (RPA), vertex (V), and ladder, particle-hole (Lph) and particle-particle (Lpp), types of diagrams

$$A_{\mu\nu(\alpha\beta)}^{\kappa\lambda,\kappa'\lambda'} = A_{\mu\nu(\alpha\beta)}^{\kappa\lambda,\kappa'\lambda'}(\text{RPA}) + A_{\mu\nu(\alpha\beta)}^{\kappa\lambda,\kappa'\lambda'}(\text{V}) + A_{\mu\nu(\alpha\beta)}^{\kappa\lambda,\kappa'\lambda'}(\text{Lph}) + A_{\mu\nu(\alpha\beta)}^{\kappa\lambda,\kappa'\lambda'}(\text{Lpp}). \tag{15}$$

The same kind of decomposition holds for all \bar{A} 's and \tilde{A} 's, appearing in Eqs. (6) and (7) in the main text respectively.

The coefficients A are therefore the sum of the following

$$A_{\mu\nu(\alpha\beta)}^{\kappa\lambda,\kappa'\lambda'}(\text{RPA}) = 2\delta_{\mu\kappa}\delta_{\nu\lambda}\delta_{\mu\kappa'}\delta_{\nu\lambda'}\text{Tr}\left((\tau_\mu\tau_\alpha)^2\right)\text{Tr}\left((\sigma_\nu\sigma_\beta)^2\right), \quad (16)$$

$$A_{\mu\nu(\alpha\beta)}^{\kappa\lambda,\kappa'\lambda'}(\text{V}) = -\frac{1}{4}\left[\delta_{\mu\kappa}\delta_{\nu\lambda}\text{Tr}\left(\tau_\kappa\tau_{\kappa'}\tau_\alpha\tau_\kappa\tau_\alpha\tau_{\kappa'}\right)\text{Tr}\left(\sigma_\lambda\sigma_{\lambda'}\sigma_\beta\sigma_\lambda\sigma_\beta\sigma_{\lambda'}\right) + \delta_{\mu\kappa'}\delta_{\nu\lambda'}\text{Tr}\left(\tau_{\kappa'}\tau_\kappa\tau_\alpha\tau_{\kappa'}\tau_\alpha\tau_\kappa\right)\text{Tr}\left(\sigma_{\lambda'}\sigma_\lambda\sigma_\beta\sigma_{\lambda'}\sigma_\beta\sigma_\lambda\right)\right], \quad (17)$$

$$A_{\mu\nu(\alpha\beta)}^{\kappa\lambda,\kappa'\lambda'}(\text{Lph}) = -\frac{1}{16}\text{Tr}\left(\tau_\mu\tau_\kappa\tau_\alpha\tau_{\kappa'}\right)\text{Tr}\left(\sigma_\nu\sigma_\lambda\sigma_\beta\sigma_{\lambda'}\right)\text{Tr}\left(\tau_\mu\tau_{\kappa'}\tau_\alpha\tau_\kappa\right)\text{Tr}\left(\sigma_\nu\sigma_{\lambda'}\sigma_\beta\sigma_\lambda\right), \quad (18)$$

$$A_{\mu\nu(\alpha\beta)}^{\kappa\lambda,\kappa'\lambda'}(\text{Lpp}) = -\frac{P_{\alpha\beta}}{32}\left[\left(\text{Tr}\left(\tau_\mu\tau_\kappa\tau_\alpha\tau_{\kappa'}\right)\text{Tr}\left(\sigma_\nu\sigma_\lambda\sigma_\beta\sigma_{\lambda'}\right)\right)^2 + \left(\text{Tr}\left(\tau_\mu\tau_{\kappa'}\tau_\alpha\tau_\kappa\right)\text{Tr}\left(\sigma_\nu\sigma_{\lambda'}\sigma_\beta\sigma_\lambda\right)\right)^2\right]. \quad (19)$$

The prefactor $P_{\alpha\beta}$ in the last equation equals +1, for $(\alpha\beta) = (01)$, (30) , or (32) , and it equals -1, for $(\alpha\beta) = (00)$, (02) , or (31) . One needs to calculate only coefficients with these $(\alpha\beta)$, since $\Phi^{(\alpha\beta)}$ is non-zero only when $\alpha = 0$ or 3 , and $\beta = 0, 1$ or 2 . This is true for all A 's, \bar{A} 's, \tilde{A} 's, α 's, and B 's, since these coefficients are always summed together with $\Phi^{(\alpha\beta)}$.

The coefficients \bar{A} are given by

$$\bar{A}_{\mu\nu(\alpha\beta)}^{\kappa,\kappa'}(\text{RPA}) = 2\delta_{\mu\kappa}\delta_{\mu\kappa'}\text{Tr}\left((\tau_\mu\tau_\alpha)^2\right)\left[\delta_{\nu 0}\text{Tr}\left((\sigma_1\sigma_\beta)^2\right) + 2\delta_{\nu 1}\right], \quad (20)$$

$$\bar{A}_{\mu\nu(\alpha\beta)}^{\kappa,\kappa'}(\text{V}) = -\frac{1}{2}\left[\delta_{\mu\kappa}\text{Tr}\left(\tau_\kappa\tau_{\kappa'}\tau_\alpha\tau_\kappa\tau_\alpha\tau_{\kappa'}\right) + \delta_{\mu\kappa'}\text{Tr}\left(\tau_{\kappa'}\tau_\kappa\tau_\alpha\tau_{\kappa'}\tau_\alpha\tau_\kappa\right)\right]\left[\delta_{\nu 0}\text{Tr}\left((\sigma_1\sigma_\beta)^2\right) + 2\delta_{\nu 1}\right], \quad (21)$$

$$\bar{A}_{\mu\nu(\alpha\beta)}^{\kappa,\kappa'}(\text{Lph}) = -\frac{1}{8}\text{Tr}\left(\tau_\mu\tau_\kappa\tau_\alpha\tau_{\kappa'}\right)\text{Tr}\left(\tau_\mu\tau_{\kappa'}\tau_\alpha\tau_\kappa\right)\left[2\delta_{\nu\beta}\text{Tr}\left((\sigma_1\sigma_\beta)^2\right) + \left(\text{Tr}\left(\sigma_1\sigma_\nu\sigma_\beta\right)\right)^2\right], \quad (22)$$

$$\bar{A}_{\mu\nu(\alpha\beta)}^{\kappa,\kappa'}(\text{Lpp}) = -\frac{P_{\alpha\beta}}{16}\left[\left(\text{Tr}\left(\tau_\mu\tau_\kappa\tau_\alpha\tau_{\kappa'}\right)\right)^2 + \left(\text{Tr}\left(\tau_\mu\tau_{\kappa'}\tau_\alpha\tau_\kappa\right)\right)^2\right]\left[2\delta_{\nu\beta}\text{Tr}\left((\sigma_1\sigma_\beta)^2\right) + \text{Tr}\left(\sigma_1\sigma_\nu\sigma_\beta\right)\text{Tr}\left(\sigma_1\sigma_\beta\sigma_\nu\right)\right]. \quad (23)$$

Finally, the coefficients \tilde{A} are the sum of the following terms

$$\tilde{A}_{\mu(\alpha\beta)}^{\kappa\lambda,\kappa'}(\text{RPA}) = 2\delta_{\mu\kappa}\delta_{\mu\kappa'}\text{Tr}\left((\tau_\mu\tau_\alpha)^2\right)\left[2\delta_{\lambda 0} + \delta_{\lambda 1}\text{Tr}\left((\sigma_1\sigma_\beta)^2\right)\right], \quad (24)$$

$$\tilde{A}_{\mu(\alpha\beta)}^{\kappa\lambda,\kappa'}(\text{V}) = -\frac{1}{4}\left\{2\delta_{\mu\kappa}\text{Tr}\left(\tau_\kappa\tau_{\kappa'}\tau_\alpha\tau_\kappa\tau_\alpha\tau_{\kappa'}\right)\left[2\delta_{\lambda 0} + \delta_{\lambda 1}\text{Tr}\left((\sigma_1\sigma_\beta)^2\right)\right] + \delta_{\mu\kappa'}\text{Tr}\left(\tau_{\kappa'}\tau_\kappa\tau_\alpha\tau_{\kappa'}\tau_\alpha\tau_\kappa\right)\left[2 + \text{Tr}\left(\sigma_1\sigma_\lambda\sigma_\beta\sigma_1\sigma_\beta\sigma_\lambda\right)\right]\right\}, \quad (25)$$

$$\tilde{A}_{\mu(\alpha\beta)}^{\kappa\lambda,\kappa'}(\text{Lph}) = -\frac{1}{8}\text{Tr}\left(\tau_\mu\tau_\kappa\tau_\alpha\tau_{\kappa'}\right)\text{Tr}\left(\tau_\mu\tau_{\kappa'}\tau_\alpha\tau_\kappa\right)\left[4\delta_{\lambda\beta} + \text{Tr}\left(\sigma_1\sigma_\lambda\sigma_\beta\right)\text{Tr}\left(\sigma_1\sigma_\beta\sigma_\lambda\right)\right], \quad (26)$$

$$\tilde{A}_{\mu(\alpha\beta)}^{\kappa\lambda,\kappa'}(\text{Lpp}) = -\frac{P_{\alpha\beta}}{16}\left\{\left(\text{Tr}\left(\tau_\mu\tau_\kappa\tau_\alpha\tau_{\kappa'}\right)\right)^2\left[4\delta_{\lambda\beta} + \left(\text{Tr}\left(\sigma_1\sigma_\lambda\sigma_\beta\right)\right)^2\right] + \left(\text{Tr}\left(\tau_\mu\tau_{\kappa'}\tau_\alpha\tau_\kappa\right)\right)^2\left[4\delta_{\lambda\beta} + \left(\text{Tr}\left(\sigma_1\sigma_\beta\sigma_\lambda\right)\right)^2\right]\right\}. \quad (27)$$

The particle-hole (p-h) instabilities are defined through Dirac bilinears, $O^i = \tau_\kappa\sigma_\lambda\delta_{\alpha\beta}$ for singlet and $O^i = \tau_\kappa\sigma_\lambda\vec{\sigma}_{\alpha\beta}$ for triplet channels. In the case of particle-particle (p-p) instabilities, Dirac bilinears corresponding to singlet channels are $\tilde{O}^i = \tau_\kappa\sigma_\lambda\sigma_{\alpha\beta}^2$, while those corresponding to triplet channels are $\tilde{O}^i = \tau_\kappa\sigma_\lambda\sigma_{\alpha\beta}^a$, with $a = 0, 1$, or 3 . The coefficients in the susceptibilities corresponding to one of these channels are

$$\alpha_{i,(\mu\nu)}^{(\text{p-h})} = 2\text{Tr}\left((\tau_\kappa\tau_\mu)^2\right)\text{Tr}\left((\sigma_\lambda\sigma_\nu)^2\right), \quad (28)$$

$$\begin{aligned} \alpha_{i,(\mu\nu)}^{(\text{p-p})} &= -\frac{(-1)^{P_{\mu\nu}}}{2}\text{Tr}\left(\tilde{O}^i(\tau_\mu\sigma_\nu\mathbb{1})\left(\tilde{O}^i - \left(\tilde{O}^i\right)^T\right)(\tau_\mu\sigma_\nu\mathbb{1})^T\right) \\ &= -2(-1)^{P_{\mu\nu}}\text{Tr}\left((\tau_\kappa\tau_\mu)^2\right)\text{Tr}\left(\sigma_\lambda\sigma_\nu\sigma_\lambda\sigma_\nu^T\right). \end{aligned} \quad (29)$$

For the p-h channels, the coefficient α depends only on κ and λ and not on whether the channel is singlet or triplet. For the p-p channels, the first line in Eq. (29) implies that only channels with antisymmetric \tilde{O}^i 's can have a non-zero susceptibility. This is already assumed in the second line of the same equation, therefore, it is applicable for singlet p-p channel susceptibilities only if $\tau_\kappa\sigma_\lambda$ is symmetric, while for triplet p-p channels it holds only if $\tau_\kappa\sigma_\lambda$ is antisymmetric. Otherwise, $\alpha^{(p-p)} = 0$. Note that we used $\tau_\mu^T = \tau_\mu$, since μ can take values 0 or 3 only.

Using the same notation, in Eq. (11) in the main text we have

$$B_{i,(\mu'\nu')}^{(p-h),\mu\nu} = 2\delta_{\mu\kappa}\delta_{\nu\lambda}\delta_i^S \text{Tr} \left((\tau_\mu\tau_{\mu'})^2 \right) \text{Tr} \left((\sigma_\nu\sigma_{\nu'})^2 \right) - \frac{1}{4} \text{Tr} (\tau_\kappa\tau_\mu\tau_{\mu'}\tau_\kappa\tau_{\mu'}\tau_\mu) \text{Tr} (\sigma_\lambda\sigma_\nu\sigma_{\nu'}\sigma_\lambda\sigma_{\nu'}\sigma_\nu), \quad (30)$$

$$\begin{aligned} B_{i,(\mu'\nu')}^{(p-p),\mu\nu} &= -\frac{(-1)^{P_{\mu'\nu'}}}{16} \text{Tr} \left(\tilde{O}^i (\tau_\mu\sigma_\nu\mathbb{1})^T (\tau_{\mu'}\sigma_{\nu'}\mathbb{1})^T \left(\tilde{O}^i - (\tilde{O}^i)^T \right) (\tau_{\mu'}\sigma_{\nu'}\mathbb{1}) (\tau_\mu\sigma_\nu\mathbb{1}) \right) \\ &= -\frac{(-1)^{P_{\mu'\nu'}}}{4} \text{Tr} (\tau_\kappa\tau_\mu^T\tau_{\mu'}\tau_\kappa\tau_{\mu'}\tau_\mu) \text{Tr} (\sigma_\lambda\sigma_\nu^T\sigma_{\nu'}^T\sigma_\lambda\sigma_{\nu'}\sigma_\nu). \end{aligned} \quad (31)$$

The symbol δ_i^S takes value 1 if O^i belongs to a singlet channel and 0 if it does not. Like before, $B^{(p-p)}$ vanishes if \tilde{O}^i is a symmetric matrix. The second line in Eq. (31) holds only for antisymmetric p-p channels.

ASYMPTOTIC BEHAVIOUR OF THE Φ 'S AND THE STABLE RAYS

We can analyse the RG flows exactly in the $\ell \rightarrow \infty$ limit. This is a consequence of the fact that Φ function in Eqs. (8) and (9) in the main text, depend only on three parameters, δ_ℓ , t_ℓ , and γ_ℓ , one of which will diverge faster than the others. Since γ_ℓ flows only by its engineering dimension -1 , Eq. (4) in the main text, the dominant diverging parameter is either t_ℓ or δ_ℓ . That single parameter determines the asymptotic behaviour of the Φ 's.

In all the flows that we studied numerically, where $0 \leq t_c \lesssim 0.1$, we always found δ_ℓ to diverge faster than t_ℓ at the phase transition. This is the case we present here. These results are applicable to $T = 0$ flows, too, since there is only one diverging parameter, δ_ℓ , in that case. We concentrate here on the case with no mixed interaction terms, $\tilde{g}_\mu = 0$, at the bare level, so none are generated during the entire RG flow.

Under the assumption that $\lim_{\ell \rightarrow \infty} t_\ell/\delta_\ell = 0$, we have

$$\Phi^{(00)} = \frac{-2}{|\delta|} + O(\delta)^{-2}, \quad \Phi^{(01)} = \frac{2}{|\delta|} + O(\delta)^{-2}, \quad (32)$$

while $\Phi^{(\mu\nu)} = O(\delta)^{-2}$ for all other $\Phi^{(\mu\nu)}$'s. Also $\Phi_0 = \text{sgn}(\delta) + O(\delta)^{-1}$. These properties allows us to write the flow equations in the large ℓ limit, and from there find all the possible stable rays along which the couplings diverge.

A ray in the coupling space is defined by the following unit vector,

$$z_{\mu\nu}(\ell) = g_{\mu\nu}(\ell) / \sqrt{\sum_{\kappa=0,3,\mathbf{K}} \sum_{\lambda=0}^3 g_{\kappa\lambda}(\ell)}, \quad (33)$$

where the summation in the denominator goes only over 12 independent coupling constants, thus $g_{\mathbf{K}\lambda} = g_{1\lambda}$ or $g_{2\lambda}$, for each λ , the two being the same according to the symmetry. A stable *diverging* ray is given by a unit vector $y_{\mu\nu}$ such that it is a fixed point for the asymptotic flow of $z_{\mu\nu}$:

$$\lim_{\ell \rightarrow \infty} \left. \frac{dz_{\mu\nu}}{d\ell} \right|_{z \rightarrow y} = 0, \quad (34)$$

while at the same time the stability matrix,

$$S_{\mu'\nu'}^{\mu\nu} = \lim_{\ell \rightarrow \infty} \frac{\partial}{\partial z_{\mu'\nu'}} \left(\frac{dz_{\mu\nu}}{d\ell} \right) \Big|_{z \rightarrow y}, \quad (35)$$

must have no positive eigenvalues.

For each particular stable ray found, it can be shown that, at the transition point, both δ_ℓ and $g_{\mu\nu}$'s diverge as $e^{(2+\eta_\delta)\ell}$, where η_δ follows from Eq. (5) in the main text,

$$\eta_\delta = \lim_{\ell \rightarrow \infty} \frac{1}{\delta_\ell} \sum_{\mu\nu} g_{\mu\nu}(\ell) C_{\mu\nu} \Phi_0(t_\ell, \delta_\ell, r_\ell). \quad (36)$$

One is then required to check if the stable ray obtained is consistent with the initial assumption of δ_ℓ diverging faster than t_ℓ . If $\eta_\delta < 0$ for any given stable ray, such a solution to Eq. (34) is violating our assumption and should be disregarded.

Using the outlined procedure, we find twelve solutions, the coupling constant stable rays, $y_{\mu\nu}$, and present them in Table II.

No.	y_{00}	y_{01}	y_{02}	y_{03}	y_{30}	y_{31}	y_{32}	y_{33}	$y_{\mathbf{K}0}$	$y_{\mathbf{K}1}$	$y_{\mathbf{K}2}$	$y_{\mathbf{K}3}$
1	0	$-\frac{1}{\sqrt{31}}$	0	0	0	0	$-\sqrt{\frac{5(6+\sqrt{35})}{62}}$	$\sqrt{\frac{5(6-\sqrt{35})}{62}}$	0	0	0	0
2	0	$-\frac{1}{\sqrt{31}}$	0	0	0	0	$\sqrt{\frac{5(6-\sqrt{35})}{62}}$	$-\sqrt{\frac{5(6+\sqrt{35})}{62}}$	0	0	0	0
3	0	$-\frac{1}{\sqrt{31}}$	$-\sqrt{\frac{5(6+\sqrt{35})}{62}}$	$\sqrt{\frac{5(6-\sqrt{35})}{62}}$	0	0	0	0	0	0	0	0
4	0	$-\frac{1}{\sqrt{31}}$	$\sqrt{\frac{5(6-\sqrt{35})}{62}}$	$-\sqrt{\frac{5(6+\sqrt{35})}{62}}$	0	0	0	0	0	0	0	0
5	0.045	-0.3723	0.1877	-0.2825	0.1394	-0.2341	0.6095	-0.3308	-0.2341	0.1394	-0.2825	0.1877
6	0.045	-0.3723	-0.2825	0.1877	0.1394	-0.2341	-0.3308	0.6095	-0.2341	0.1394	0.1877	-0.2825
7	0.045	-0.3723	0.6095	-0.3308	0.1394	-0.2341	0.1877	-0.2825	0.1394	-0.2341	0.1877	-0.2825
8	0.045	-0.3723	-0.3308	0.6095	0.1394	-0.2341	-0.2825	0.1877	0.1394	-0.2341	-0.2825	0.1877
9	0	$-\frac{1}{\sqrt{14}}$	0	0	$\frac{1}{\sqrt{14}}$	0	0	0	0	0	$-\frac{3+\sqrt{15}}{2\sqrt{14}}$	$-\frac{-3+\sqrt{15}}{2\sqrt{14}}$
10	0	$-\frac{1}{\sqrt{14}}$	0	0	$\frac{1}{\sqrt{14}}$	0	0	0	0	0	$\frac{-3+\sqrt{15}}{2\sqrt{14}}$	$-\frac{3+\sqrt{15}}{2\sqrt{14}}$
11	$-\frac{1}{2\sqrt{38}}$	$-\frac{5}{2\sqrt{38}}$	$\frac{\sqrt{15}}{2\sqrt{38}}$	$-\frac{\sqrt{15}}{2\sqrt{38}}$	$\frac{3}{2\sqrt{38}}$	$\frac{3}{2\sqrt{38}}$	$-\frac{\sqrt{15}}{2\sqrt{38}}$	$\frac{\sqrt{15}}{2\sqrt{38}}$	$-\frac{3}{2\sqrt{38}}$	$-\frac{3}{2\sqrt{38}}$	$\frac{\sqrt{15}}{2\sqrt{38}}$	$-\frac{\sqrt{15}}{2\sqrt{38}}$
12	$-\frac{1}{2\sqrt{38}}$	$-\frac{5}{2\sqrt{38}}$	$-\frac{\sqrt{15}}{2\sqrt{38}}$	$\frac{\sqrt{15}}{2\sqrt{38}}$	$\frac{3}{2\sqrt{38}}$	$\frac{3}{2\sqrt{38}}$	$\frac{\sqrt{15}}{2\sqrt{38}}$	$-\frac{\sqrt{15}}{2\sqrt{38}}$	$-\frac{3}{2\sqrt{38}}$	$-\frac{3}{2\sqrt{38}}$	$-\frac{\sqrt{15}}{2\sqrt{38}}$	$\frac{\sqrt{15}}{2\sqrt{38}}$

TABLE II: Twelve stable rays.

In Table II, $y_{\mu\nu}$ for rays Nos. 5-8 are given by their numerical value, but can be obtained in a closed form in terms of zeros of a fourth order polynomial. For example, along the stable ray No. 8, the ratio $\omega = y_{02}/y_{03}$ is a particular zero (≈ -0.5427) of polynomial

$$0 = 7127\omega^8 + 31470\omega^7 + 61602\omega^6 + 91050\omega^5 + 109022\omega^4 + 91050\omega^3 + 61602\omega^2 + 31470\omega + 7127. \quad (37)$$

This polynomial is symmetric and can be reduced to a fourth order polynomial by a division by ω^4 and substitution $z = \omega + 1/\omega$. Therefore, there is a closed form solution for ω which is an algebraic number. The other ratios are then related to ω as

$$\begin{aligned} \frac{y_{00}}{y_{03}} &= \frac{9 + 14\omega + 9\omega^2 - \Xi}{8(1 + \omega)}, & \frac{y_{01}}{y_{03}} &= \frac{-3 + 22\omega - 3\omega^2 + 3\Xi}{16(1 + \omega)}, & \frac{y_{30}}{y_{03}} &= \frac{y_{\mathbf{K}0}}{y_{03}} = \frac{1 + \omega}{2}, \\ \frac{y_{31}}{y_{03}} &= \frac{y_{\mathbf{K}1}}{y_{03}} = \frac{(1 - \omega)^2 - \Xi}{8(1 + \omega)}, & \frac{y_{32}}{y_{03}} &= \frac{y_{\mathbf{K}2}}{y_{03}} = \frac{(1 + 3\omega)^2 - \Xi}{16(1 + \omega)}, & \frac{y_{33}}{y_{03}} &= \frac{y_{\mathbf{K}3}}{y_{03}} = \frac{(3 + \omega)^2 - \Xi}{16(1 + \omega)}, \end{aligned} \quad (38)$$

where $\Xi = (33 + 60\omega + 70\omega^2 + 60\omega^3 + 33\omega^4)^{1/2}$. In phases Nos. 5-7, the values for the ratios are given by a permutation of the No. 8 stable ray ratios.

The properties of the instabilities associated with each stable ray are listed in Table III. We give the name to each phase, list the order parameter of the leading instability, the IR that the order parameter transforms according to, whether it is even (+) or odd (-) under the time reversal symmetry (Θ), if it is gapped or not, and give η_δ . The instabilities with order parameter transforming according to an IR at Γ point have a spatially uniform order parameter. The two instabilities with the order parameter transforming according to IR's at $\pm\mathbf{K}$ represent *lattice commensurate* density waves.

For the cases of interaction considered in the main text we found flows to go into one of the following phases: MB, AF, QSH, LPDW, and s_{++} -SC. In the case of the attractive Hubbard interaction, we found the flow to go toward a ray obtained from the AF stable ray, Table II, phase No. 8, by keeping y_{01} , y_{30} , y_{32} , y_{33} , and $y_{\mathbf{K}1}$ the same and reversing the signs of all other $y_{\mu\nu}$'s. This ray is fixed (Eq. (34) holds), but unstable and is a consequence of fine tuning of the interaction.

No.	Name	O_i	IR	Θ	Gapped	η_δ
1	Mirror breaking (MB)	$\tau_3\sigma_21$	$A_{2q,\Gamma}^+$ -singlet	+	N	1/3
2	Quantum anomalous Hall (QAH)	$\tau_3\sigma_31$	$A_{2q,\Gamma}^-$ -singlet	-	Y (in bulk)	1/3
3	Inversion breaking (IB)	$1\sigma_21$	$A_{2u,\Gamma}^-$ -singlet	-	N	1/3
4	Layer polarized (LP)	$1\sigma_31$	$A_{2u,\Gamma}^+$ -singlet	+	Y	1/3
5	Triplet mirror breaking (tMB)	$\tau_3\sigma_2\vec{\sigma}$	$A_{2q,\Gamma}^-$ -triplet	-	N	0.4622
6	Quantum spin Hall (QSH)	$\tau_3\sigma_3\vec{\sigma}$	$A_{2q,\Gamma}^+$ -triplet	+	Y (in bulk)	0.4622
7	Triplet inversion breaking (tIB)	$1\sigma_2\vec{\sigma}$	$A_{2u,\Gamma}^+$ -triplet	+	N	0.4622
8	Layer anti-ferromagnet (AF)	$1\sigma_3\vec{\sigma}$	$A_{2u,\Gamma}^-$ -triplet	-	Y	0.4622
9	Interlayer current density wave (ICDW)	$\tau_1\sigma_21$ or $\tau_2\sigma_21$	$A_{2,\pm\mathbf{K}}^-$ -singlet	-	N	7/16
10	Layer polarization density wave (LPDW)	$\tau_1\sigma_31$ or $\tau_2\sigma_31$	$A_{2,\pm\mathbf{K}}^+$ -singlet	+	N	7/16
11	s_{++} -superconducting (s_{++} SC)	$\tau_11\sigma_2$ (p-p)	$A_{1q,\Gamma}^+$ -singlet	+	Y	7/16
12	Interlayer pairing superconducting (i SC)	$\tau_1\sigma_1\sigma_2$ (p-p)	$A_{1q,\Gamma}^+$ -singlet	+	N	7/16

TABLE III: The list of all the possible phases in TLG with their properties.